Journal of Dentistry 130 (2023) 104447

Contents lists available at ScienceDirect

Journal of Dentistry

journal homepage: www.elsevier.com/locate/jdent

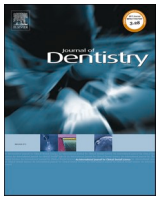

Dexamethasone-doped nanoparticles improve mineralization, crystallinity and collagen structure of human dentin

Manuel Toledano, Estrella Osorio, María T. Osorio, Fátima S. Aguilera *, Raquel Toledano, Enrique Fernández- Romero, Raquel Osorio

Faculty of Dentistry, Dental Materials Section, Colegio Máximo de Cartuja s/n, University of Granada, Granada 18071, Spain

ARTICLE INFO

Keywords:
Dentin
Dexamethasone
Nanoparticles
Mechanical
Raman
Remineralization

ABSTRACT

Objectives: Bioactive materials have been used for functionalization of adhesives to promote dentin remineralization. This study aims to evaluate bonding ability and both mechanical and chemical behavior of demineralized dentin infiltrated with polymeric nanoparticles doped with dexamethasone (Dex-NPs).
Methods: Dentin conditioned surfaces were infiltrated with NPs, Dex-NPs or Dex-Zn-NPs. Bonded interfaces were also created and stored for 24 h or 21d, and then submitted to microtensile bond strength testing. Dentin remineralization was analyzed by Nanohardness, Young's modulus and Raman analysis.
Results: At 21d of storage, dentin treated with undoped-NPs attained the lowest nanohardness and Young's modulus. Dex-NPs and Zn-Dex-NPs increased dentin nanohardness and Young's modulus after 21d Raman analysis showed high remineralization, crystallinity, crosslinking and better structure of collagen when functionalized Dex-NPs were present at the dentin interface.
Conclusions: Infiltration of dentin with Dex-NPs promoted functional remineralization as proved by nanomechanical and morpho-chemical evaluation tests. Dexamethasone in dentin facilitated crystallographic maturity, crystallinity and improved maturity and secondary structure of dentin collagen.
Clinical significance: Using dexamethasone-functionalized NPs before resin infiltration is a clear option to obtain dentin remineralization, as these NPs produce the reinforcement of the dentin structure, which will lead to the improvement of the longevity of resin restorations.

1. Introduction

Strong and durable adhesion to dentin is one of the main goals in the modern operative dentistry [1]. Dentin is a compound of nanocrystals of hydroxyapatite and collagen molecules [2]. In adhesive dentistry, "Etch-and-rinse" adhesives represent the gold standard [3]. This technique involves a previous phosphoric acid conditioning to demineralize the dentin before the placement of the adhesive resin. The created interface is the hybrid layer, made of collagen and resin [2,4]. A three-dimensional resin-collagen biopolymer providing both an stable and continuous link between the dentin substrate and the bulk adhesive characterizes the ideal hybrid layer [5]. Nevertheless, a fraction of demineralized/unprotected collagen appears at the bottom of the hybrid layer, prone to degradation by matrix or bacterial collagenases [6], and should be remineralized [7,8].

When formulating dental adhesives, protection of demineralized collagen fibers and long-lasting adhesion to dentin, are perused [9]. In order to facilitate mineral precipitation within the hybrid layer and further remineralization of the underlying dentin, bioactive materials have been proposed for functionalization of adhesives [10]. These biomaterials have contributed to the regrowth of minerals at the demineralized dentin, but they do not have an ideal degradation kinetics nor a well-regulated release [11]. The role of corticoesteroids in hard tissues has attracted some attention. Due to the permeability of dentin, medication molecules as corticoesteroids, placed on the exposed dentin, diffuse through the dentin substrate and tubules, with the potential to produce a therapeutic effect within the dentin [12]. Dexamethasone (Dex) is a powerful synthetic glucocorticoid clinically used as an anti-inflammatory drug [13]. It has been employed as a bioactive molecule for hard tissues [14], and to increase mineralization and expression of odontogenic markers in cultured stem cells from apical papilla [15]. The amount of dosed corticosteroid may be important in its

* Corresponding author.
E-mail address: fatimas@ugr.es (F.S. Aguilera).

https://doi.org/10.1016/j.jdent.2023.104447
Received 7 November 2022; Received in revised form 1 February 2023; Accepted 4 February 2023
Available online 6 February 2023

clinical result [16]. When used at high doses and for long term therapy, Dex exerts adverse effects. Because of this, it is favored the use of Dex through incorporation into biomaterials [14]. Within this purpose, Dex has been previously integrated within composite nanofibers [17]. Local small doses of Dex, over months, were delivered by a system designed by Lim et al. [14]. Cellular responses in vitro and/or improvement of in vitro tissue healing with little side effects have been reported after stimulating many other local delivery systems of Dex [18]. Porous bio-sponges consisting of high deacetylated chitosan and collagen type-1 loaded with Dex have also been fabricated to stimulate calcification of dentin [13].

In order to mimic the nanoscale structure of native extracellular matrix, nanoparticles (NPs) have been recently developed as promising tools for formulating biomimetic materials to encourage regeneration of tissues [19]. Hydrophilic polymeric NPs represent a highly qualified drug carrier due to their favorable biocompatibility, high loading capacity and great specific surface areas. Non-resorbable polymeric NPs loaded with reinforcing agents and antimicrobials have successfully been tested previously [20–22], but it has been very sparsely considered the combined anti-inflammatory therapy. Novel polymeric NPs with anionic carboxylate (*i.e.,* COO−) groups on the backbone of the polymer, have been previously synthesized and loaded with calcium (Ca-NPs), zinc (Zn-NPs), doxycycline (D-NPs), melatonine (ML-NPs) to favor dentin remineralization [21–23]. Dex, which could promote the osteoblast differentiation enhancing bone remineralization and the alkaline phosphatase activity [19], has been loaded into carboxylated NPs to be applied in dentin to be remineralized, in the present research.

A boost to innovation and a breakthrough in dental regenerative biomaterials is represented by the incorporation of zinc (Zn) into polymeric NPs. At the bonded interface, Zn does induce dentin remineralization, influencing signaling pathways [24,25]. In addition, Zn reduces matrix metalloproteinases (MMPs)-mediated collagen degradation [26], inhibiting dentin demineralization [27], thereby preserving hydroxyapatite (HAp). Biological apatite contains substantial amounts of carbonate and is calcium deficient. In the presence of Zn, an exchange between Zn^{2+} and Ca^{2+} occurs in vitro forming a substituted apatite compound in the carbonated apatite, that is a precursor of HAp [28]. Akin to bone [29], it derives its mechanical performance from the shared contributions of these elements and their structural measures over length scales oscillating from the nano- to the microscale [30]. The most used applied means of testing the mechanical properties of materials or substrates is nanoindentation [31]. Furthermore, Raman spectroscopy and cluster analysis offer non-destructive measurements, providing an insight on molecular structure, biochemical nature and emission spectroscopies of the tissue. The number of molecules within the volume of the scanned area is proportional to the Raman peak intensity [32].

In order to elucidate and confirm its therapeutic role in dentin strengthening, Dex-NPs application on dentin surfaces has been tested throughout both nano-mechanical tests and Raman analysis. The aim of this study was to investigate the effect of dexamethasone-loaded NPs (Dex-NPs) and dexamethasone-loaded/Zn-doped NPs (Zn-Dex-NPs) application on the mid-term stability of these resin-dentin interfaces and dentin remineralization. Mechanical and chemical properties, bonding efficacy and histo-morphological changes after treating dentin surfaces with Dex-NPs and Zn-Dex-NPs have been studied. The tested null hypothesis was that dexamethasone-doped NPs application did not affect, at the short term or overtime, dentin remineralization expressed in terms of bonding efficacy, morphological characteristics, mechanical and biochemical properties.

2. Materials and methods

2.1. Nanoparticles fabrication and characterization

The polymerization precipitation method was used to obtain nanoparticles (NPs). A thermo-dynamic approach allowed controlling the precipitation process, that is, the Flory-Huggins model based on Hansen's solubility parameters. This model was based on the solvent molecules interactions and the growth of the polymer chains by hydrogen, polar bonding and dispersion forces [33]. The backbone monomer used for the NPs design was 2-hydroxyethyl methacrylate, the functional monomer was methacrylic acid, and ethylene glycol dimethacrylate was used as cross-linker. Finally, NPs were loaded with Dex and Zn^{2+}. The NPs Dex and Zn loading process was achieved via immersion of 30 mg of NPs in an aqueous solution of $ZnCl_2$ (40 mg/L, phosphate buffer pH=7) or Dexamethasone (40 mg/L, phosphate buffer pH=7). NPs were maintained for 4 h under constant shaking (rotator Orbit 300,445, JP Selecta, Barcelona, Spain) at 12 rpm. The NPs were then centrifuged (Centrofriger BLT, JP Selecta, Barcelona, Spain) at 6000 rpm for 30 min and the particles were separated from the supernatant and washed. The same centrifugation procedure was repeated twice, adding PBS solution for washing purposes. Finally, the NPs were separated from the supernatant and dried in an oven at 45 °C (Selecta, JP Selecta, Barcelona, Spain) until constant weight. Four experimental groups were formed: 1) control, 2) undoped-NPs, 3) Dex-NPs and 4) Zn-Dex-NPs, where a mixture of 50% of Zn-NPs and 50% of Dex-NPs was created.

For size and Z-potential measurements, a 5 mg/mL suspension of Dex-NPs in water was fixed. These analyses were also prepared in triplicate using a Zetasizer Nano ZS90 (Malvern Instrument Ltd, Malvern, UK) via dynamic light scattering (DLS).

NPs TEM characterization was also performed by placing 10μL of diluted samples (1 mg/mL) on a copper grid; then, it was coated with activated carbon and next dried. The samples were negatively stained with uranyl acetate at 2%, for visualization [34,35]. A Fei Titan 80–300 TEM-STEM microscope (ThermoFisher Scientific, Waltham, USA) was employed to acquire images (at 300 kV).

For Fourier-transform infrared spectroscopy (FTIR) characterization, NPs, Dex-NPs and Zn-Dex-NPs samples were exposed to a JASCO 6200 FTIR equipped with a diamond-tipped attenuated total reflectance (ATR) device (ATR Pro-ONE, JASCO Inc., Maryland, USA). The frequency range was 400–4000cm^{-1}, and the spectral resolution, 2cm^{-1} during 75 scans. Samples did not require preparation to obtain the spectra, minimizing artifacts [36].

2.2. Specimens' preparation for microtensile bond strength (MTBS)

Thirty-two extracted unerupted human third molars, which had previously been stored at 4 °C in a 0.5% chloramine T solution for a period no longer than 1 month, were used. Before subjects' participation and inclusion in the study, informed consent was obtained. The study conformed to the Declaration of Helsinki and was performed to the guidelines of good clinical practice. Ethical approval for the study involving human subjects was granted by the Institutional Ethics Committee on Human Research (1906/CEIH/2020).

Teeth were sectioned horizontally just below the dentin-enamel junction to obtain sound dentin surfaces. These surfaces were polished flat to acquire a clinically relevant smear layer, using 180-grit silicon carbide –SiC- abrasive paper. Dentin surfaces were then etched with 37% phosphoric acid, for 15 s, rinsed by air-water spraying for 30 s and dentin blotting with absorbent paper to keep the surface visibly moist. The experimental teeth were randomly allocated to one of the eight groups ($n = 4$ teeth) by means of a computer generated randomization list, according to the type of NP and storage time employed. The research random assignment tool used was http://www.randomizer.org/form.htm, and the teeth allocation to the treatment was concealed by means of sealed envelopes until the time of the bonding procedure. Just an ethanol solution was applied (30 s) (*i*), or an ethanol suspension of undoped-NPs (*ii*), Dex-NPs (*iii*), and Zn-Dex-NPs (*iv*) (1 mg/mL) in each of the four experimental groups, acting as primers. Ethanol was then evaporated for 30 s and, finally, Single Bond (SB) resin (3 M ESPE, St. Paul, MN, USA) was applied according to the manufacturer's instructions, to fulfill the conventional adhesive protocol. The sample

preparation was always done by the same researcher (E.F.) and the adhesion protocol was undertaken by another distinct researcher (F.S. A.). For each tooth, a composite build-up (6 mm high) (Tetric EvoCeram, Ivoclar-Vivadent, Schaan, Liechtenstein) was constructed using the incremental technique, in six 1 mm resin layers, and light-cured with a Bluephase® polywave light-emitting diode light-polymerizing unit (Bluephase G2, Ivoclar Vivadent AG, Schaan, Liechtenstein) for 20 s. The output intensity was monitored with a curing radiometer (Model Bluephase® meter, Ivoclar Vivadent AG, Schaan, Liechtenstein). A minimal output intensity of 1000 mW/cm^2 was employed for the experiments. Half of the restored teeth were stored in a dark environment in simulated body fluid solution (SBFS) for 24 h (n = 4, from each experimental group), and the other half for 21d (n = 4, from each experimental group) at 37 °C. These bonded teeth were sliced into beams with a cross-section of 1mm^2, providing approximately 10 sticks per tooth. In total, 320 beams were scored in the present research, 160 beams were analyzed at 24 h and another 160 specimens at 21d Thus, 40 specimens were obtained for each dentin treatment/storage time group. Each beam was fixed to a modified Bencor Multi-T testing device (Danville Engineering Co., Danville, CA, USA). Specimens were carefully aligned and a gel-like command-set glue (Zapit, Dental Ventures of America, Corona, CA, USA) was used, as it permits a controlled application sufficiently remote from the adhesive interface. Therefore, the specimens were aligned in the soft glue gel prior to the application of the hardener (spray) to cure. Sticks were then assayed for failure in tension at a crosshead speed of 0.5 mm/min by a universal testing machine (Instron 4411; Instron Corporation, Canton, MA, USA). A set of 2 digital calipers (Sylvac Ultra-Call III, Fowler Co., Inc., Newton, MA, USA) with an accuracy of 0.01mm^2 were used to measure the cross-sectional area at the failure site. Specimen failures which occurred at any moment during samples preparation or testing are considered pre-testing failures. They were explicitly noted as "pre-failed sticks" in Table 1 but excluded from the statistical analysis. Values were calculated in MPa and, afterwards, analyzed by ANOVA and Student-Newman-Keuls multiple comparisons (p<0.05), by the software SPSS/PC+. A stereomicroscope (Olympus SZ-CTV; Olympus, Tokyo, Japan) was employed to define failure mode of fractured specimens at 40X magnification. Failure modes were categorized as cohesive (C), mixed (M) or failure adhesive (A). To analyze the dentin sticks by field emission scanning electron microscopy (FESEM) (Gemini, Carl Zeiss, Oberkochen, Germany) at an accelerating voltage of 3 kV, detached dentin beams were selected and submitted to a critical drying point and, finally, coated with carbon.

Table 1
Mean and standard deviation (SD) of microtensile bond strength (MTBS) (MPa) to dentin and mode of failure in each of the experimental groups, after different storage times (n = 40).

Dentin Treatment	Mean (SD) [pre-failed sticks] (Adhesive/Mix/Cohesive failure-%-)	
	24h	21d
Control (PA+SB)	28.90 (7.30) a1[2] (0/100/0)	17.71 (4.62) a1[3] (20/80/0)
PA +undoped NPs+SB	17.82 (6.23) a1[4] (10/90/0)	19.63 (7.76) a1[5] (15/85/0)
PA +Dex-NPs+SB	20.18 (5.93) a1[2] (18/82/0)	22.51 (8.40) a1[0] (7/90/3)
PA +Zn-Dex-NPs+SB	26.07 (7.88) a1[0] (10/90/0)	19.55 (4.57) a1[0] (5/90/5)

Abbreviations: MTBS: microtensile bond strength to dentin; SD: standard deviations; PA: Phosphoric Acid; SB: Single Bond adhesive system; NPs: nanoparticles; Dex: Dexamethasone.
For each vertical column, same letter indicates no significant differences between treatment groups within the same storage period. For each row, same number indicates no significant differences between the storage periods (24 h or 21 days) in the same treatment group (p>0.05). Number of pre-failed sticks is between brackets; percent of mode of failures are expressed as: (Adhesive/Mix/Cohesive).

2.3. Specimens' preparation for mechanical and chemical characterization of treated dentin

Twenty human third molars, without caries lesions and extracted for surgical reasons, were obtained after informed consent from donors (age: 20–40 years), within the protocol approved by the Institutional Ethics Committee on Human Research (1906/CEIH/2020). Specimens were randomly consigned to four groups (n = 5) according to the type of NP employed. To expose the flat surfaces of sound coronal dentin, a hard tissue microtome (Accutom-50; Struers, Copenhagem, Denmark) with a slow-speed, water-cooled diamond wafering saw (330-CA RS-70,300; Struers) were used. To produce one dentin disk (2.5-mm thick) per tooth, molars were transversally divided (Isomet 4000: Buehler Ltd., Lake Bluff, IL, USA), at the mid-coronal portion of each tooth. SiC abrasive papers from 800 up to 4000 grit, and a final polishing procedure with diamond pastes until 0.1 μm (Buehler-MetaDi; Buehler Ltd.) were used to polish these discs. The samples were cleaned (ultrasonic bath model QS3; Ultrawave Ltd., Cardiff, UK) at each polishing step for 5 min with deionized water (pH 7.4).

2.3.1. Nanoindentation

Using the same specimens described above, nanoindentation process was performed by means of Hysitron Ti 950 nanoindenter (Hysitron, Inc., Minneapolis, MN). The Berkovich (three-sided pyramidal) diamond indenter tip (tip radius ~20 nm) was calibrated against a fused quartz sample (quasistatic force setpoint of 5μN). On each dentin specimen, ten indentations (peak of load of 4,000μN, time function of 10 s) were performed at intertubular dentin at 24 h and 21d of storage. The process was executed in a hydrated condition by the application of a ethylene glycol layer over the specimen surface, avoiding water evaporation during a characteristic 25-to-30-min scanning period [37]. The distance between each indentation was kept constant in 5(±1)μm [25]. Nanoindentation modulus (*Ei*) and nanohardness (*Hi*) of the samples were obtained from this test. By the application of the Oliver-Pharr theoretical model, Young's modulus was obtained [38]. This method is based on a continuum, isotropic, homogeneous elastic contact model to determine the reduced modulus, *Er*. The load (*F*) was obtained as a function of the penetration depth (*h*) of the indenter in the sample. To obtain *Er*, the slope (*S*) of the unloading portion of the load-*vs*-depth data was used according to the following equation [38]:

$$S = \frac{dF}{dh} = \frac{2}{\sqrt{\pi}} E_r \sqrt{A}, \quad (1)$$

where A is the projected contact area of the hardness impression of the indenter. Then, *Ei* of the sample is obtained through the following expression:

$$\frac{1}{E_r} = \frac{\left(1 - v_{ind}^2\right)}{E_{ind}} + \frac{\left(1 - v_i^2\right)}{E_i}, \quad (2)$$

In this expression "*i*" subscript refers to the tested sample and "*ind*" subscript to the indenter. v is the Poisson's ratio and E is the Young's modulus. For hard materials as dentin, usually $E_{ind} >> E_i$ and consequently the contribution of the indenter in Eq. (2) can be neglected. Using the software Triboscan Quasi version 8.4.2.0 (Hysitron, Inc., Minneapolis, USA) Young's modulus was automatically calculated. The rest of the procedures were in Oliver and Pharr (1992) and Toledano et al. (2017). Kolmogorov-Smirnov and Levene's tests were used for data normality and homogeneity of variance assumptions (p > 0.05). Data were analyzed by two-way ANOVA including interactions. NPs application and storage time were independent factors. Student-Newman-Keuls was used for multiple comparisons (p<0.05). Student *t*-test was performed for comparisons between storage times within the same NPs application group (p<0.01).

2.3.2. Raman spectroscopy

A Raman spectrometer/microscope (Xplora, Horiba Scientific, Villeneuve d'Ascq, France) was used for Raman analysis on the same dentin surfaces. The microscope was equipped with a 100X objective and a 785-nm diode laser. A 600 lines/mm graft, that was centered between the wavelengths of 400 and 1700cm^{-1}, acquired the Raman signal.

For each dentin sample, two mappings of 12×12 μm area were performed at different positions, with a spacing between each point of 0.5 μm (for both X and Y axes). For each mapping, using the multivariate analysis tool (ISys® Horiba), a K-means cluster analysis (KMC) was performed, which includes a statistical pattern to generate independent clusters. The software to classify different natural groups of components used Hierarchical Cluster Analysis (HCA). This analysis is employed in spectroscopy to classify spectra of a dataset into component groups (or clusters) having similar spectral properties. As the centroids of the clusters are essentially means of the cluster elements score, both organic and mineral nature components were verified for each cluster. For each mapping 625 spectral points were collected. Clusters were established following Ward's technique and the dendrogram was obtained by applying three factorial spectra or principal components, representing three different constituents for the dentin surface (red, blue, and green). At this moment, the mineral (relative presence of minerals and crystallinity) and organic components (normalization, crosslinking, nature and secondary structure of collagen, and proteoglycans) of dentin were calculated.

Relative presence of mineral:

1. *Phosphate* (960cm^{-1}) *and carbonate* (1070cm^{-1}) *peaks and areas of their bands*. Peaks intensity was processed in absorbance units, *i.e.*, in arbitrary units, or counts.
2. *Relative mineral concentration* (RMC) (*i.e.*, mineral-to-matrix ratio). This index is obtained from the ratio of the peaks intensities at 960cm^{-1} (phosphate) $\nu1(PO_4^3)$ and 1003cm^{-1} (phenyl group), the aromatic ring of phenylalanine residues in collagen. This ratio indicates the maximum relative degree of mineralization [39,40].
3. Stoichiometric HAp is related to phosphate $\nu1$ vibration, located at 963cm^{-1} [41].
4. MMR is the relative mineral content or the degree of demineralization based on spatial position. This index is obtained from the ratios associated with mineral $\nu1$ [960cm^{-1}] and CH_2 deformation of collagen [1450cm^{-1}] [42].

Crystallinity:

1. FWHM: It was evaluated based on the Full Width at Half Maximum of the phosphate band at 960cm^{-1} and carbonate band at 1070cm^{-1}. These indexes expressed the crystallographic or relative atomic order, since narrower peaks suggest less structural variation in bond distances and angles [40] In general, the narrower the spectral peak width is, the higher the degree of mineral crystallinity [39].
2. Ratio 1020/1030: These intensities ratio express the crystallinity of biological apatites (1020cm^{-1}, nonstoichiometric apatites containing HPO_4^{2-}, CO_3^{2-}, and vacancies; 1030cm^{-1}, stoichiometric apatites) [43].

The dentin organic component was examined analyzing the following parameters:

Normalization: Phenyl group; it is assigned to the C—C bond of the phenyl group. For normalization, the peak at 1003cm^{-1} is noted [44].

Crosslinking: Pyridinium ring vibration; the peak that appeared at 1030/1032.7cm^{-1} of the spectra is attributed to the C—C vibration of the pyridinium ring which has a trivalent amino acid cross-linking residue [45]. The crosslinking formation is denoted by a relative intensity increase in this peak [46].

Nature and secondary structure of collagen:

1. Amide I, CH_2 and amide III; the peaks at 1655/1667, 1450 and 1246/1270cm^{-1}, assigned to amide I, CH_2 and amide III, respectively, express the molecular conformation of the polypeptide chains [44,46]. Damage or removal of collagen fibrils are indicate by the decrease of amide I peak [47]. In general, 1450cm^{-1} (CH deformation bands) is associated with proteins, lipids and carbohydrates; it is in line with the immature stage [48].
2. C—C stretch hydroxyproline is assigned to peak at 871cm^{-1} [41].
3. The bands corresponding to the vibrations at 920cm^{-1} are linked to the hydroxylated proline (P-OH stretching and ν(C—C) [49].
4. At 937cm^{-1} band, there are expressed the intensities of collagen (proline/hydroxyproline/C—C skeletal of collagen backbone) [50].
5. The peak at 1340cm^{-1} is assigned to protein α-helices, which is dependent on molecular orientation [51].
6. Proteoglycans are found at 1062cm^{-1} [50] and they are sensitive to the mechanical and structural integrity of the tissue [52].
7. Lipids; detection of bands of phospholipids and extracellular lipids at 1465 and 1440cm^{-1}, highlights the presence of cell membrane debris, which have a major role at the early stage of hard tissues maturation or healing [53].

3. Results

3.1. Fabrication and characterization of nanoparticles

The diameter of unloaded-NPs was 242.3 ± 20 nm. The zeta potential was −38.5 ± 1.0 mV. The size of Dex-NPs measured by DLS was 247.7 ± 34.26 nm in diameter. The zeta potential was −16.77±0.15 mV. The hydrodynamic diameter of Zn-NPs was 240±30 nm with a potential zeta of −41±5 mV. Fig. 1 shows TEM images of NPs. NPs did not agglomerate and presented a roughly spherical shape. After Dex or Zn-Dex loading, no differences were found in morphology.

The FTIR spectra of undoped-NPs (Fig. S1A), Dex-NPs (Fig. S1B) and Zn-Dex-NPs (Fig. S1C), had the same number of bands because the binding of dexamethasone and Zn to the NPs did not provide new functional groups that can give rise to different vibrational modes. On the other hand, a change in the intensities of some bands can be observed between the spectra of undoped-NPs and Dex-NPs, which may be due to the functional groups of NPs (ROH, OCR_2, and RCOOH), and the hydrogen bond interactions between the functional groups of Dex (ROH, OCR_2, and RCOOH).

3.2. Microtensile bond strength (MTBS) testing

Table 1 summarized means bond strength attained for each experimental group. Among groups, no differences were found. Recorded failures were mainly mixed in all experimental groups (Table 1).

SEM analysis of debonded interfaces permit to observe that after 21d of SBFS storage, residual resin partially infiltrated the dentin surface (Fig. S2B). Mineral precipitation occurred at both intertubular and peritubular dentin after using undoped-NPs (Fig. S3B). These minerals adopted a net-shaped morphology when NPs were doped with dexamethasone (Fig. 2B). Profuse resin infiltration and strong pattern of dentin remineralization were adverted after using Zn-Dex-NPs (Fig. 3B).

3.3. Mechanical and chemical characterization of treated dentin

NPs application ($p < 0.05$) and storage time ($p < 0.05$) influenced Nanohardness, *Hi*, of the dentin surfaces. Interactions among factors were significant ($p < 0.05$). Mean and SD of *Hi* are represented in Fig. 4A. At 24 h time point, untreated dentin showed the highest *Hi*, and the other three groups, that employed NPs, performed similar. *Hi* decreased overtime in the untreated dentin. When undoped-NPs were used, *Hi* did not change after 21d of storage, and *Hi* augmented over time when both Dex-NPs and Zn-Dex-NPs were employed. At 24 h time point, both untreated dentin and dentin treated with undoped-NPs showed the highest

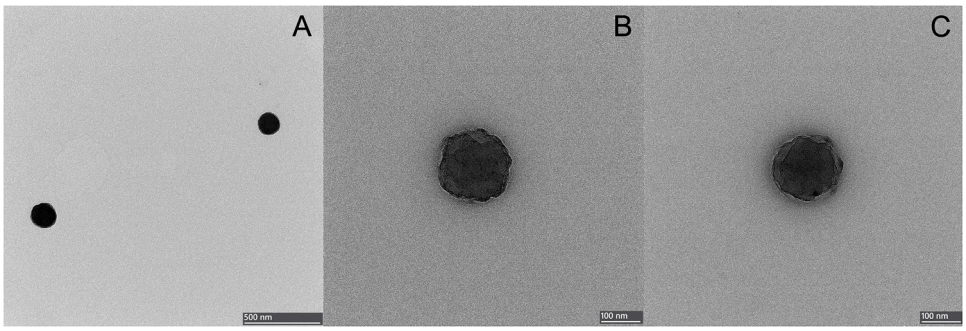

Fig. 1. Transmission electron microscopic (TEM) images of undoped-nanoparticles (undoped-NPs) (A), dexamethasone-doped NPs (Dex-NPs) (B) zinc-doped NPs (Zn-NPs) (C). Dark and light objects inside the NPs were artifacts that developed during electron beam transmission. Scale bars are 500 nm (A) and 100 nm (B, C).

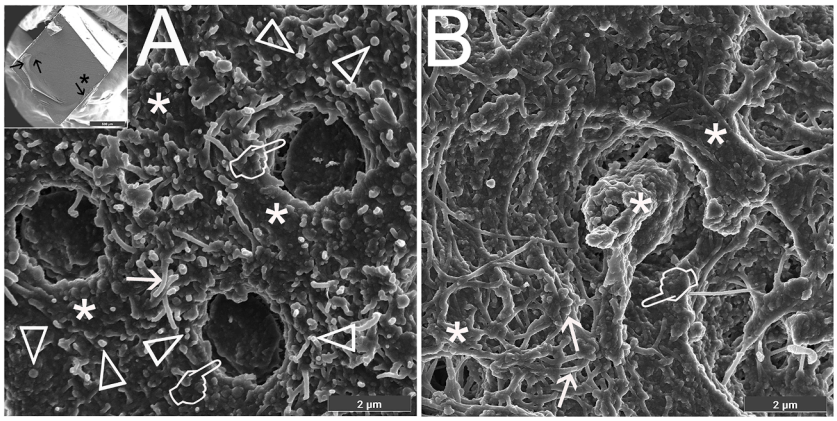

Fig. 2. SEM observations of the fractured dentin surface bonded with Dex-NPs and Single Bond adhesive (Dex-NPs group) after 24 h (A) and 21d (B) SBFS immersions. A, Mixed failure and fracture at the bottom of hybrid layer may be observed. At higher magnification, collagen fibers are clearly observed at intertubular dentin, some of them partially mineralized, or resin-infiltrated, permitting to observe the presence of mineral crystals embedded in a remnant resin/collagen scaffold-like structure. (arrows). NPs attached to demineralized collagen (faced arrows). Extensive zones of resin-infiltrated dentin were shown (asterisks). Enlarged and not completely sealed tubule entrances were also apparent. Non adapted resin tags appeared filling the tubules (pointers). Inset: A generalized mixed failure is shown. Main fracture is at the top of the hybrid layer [remaining scratches from the surface preparation may be observed (asterisk)]. Some zones showed the remained adhesive layer (arrows). B, After 21d of storage, a mixed failure of the hybrid layer was observable. Net-shaped precipitated crystals appeared covering the intertubular and peritubular dentin (asterisks). A first layer of crystal nucleation may be detected throughout the net (pointer). Crystals nucleated coating the collagen fibrils and permitting the observation of the mineralized collagen web (arrows). Remineralized NPs were adverted (arrowheads). Magnification: (A) 55,000X; (inset A) 300X; (B) 55,000X.

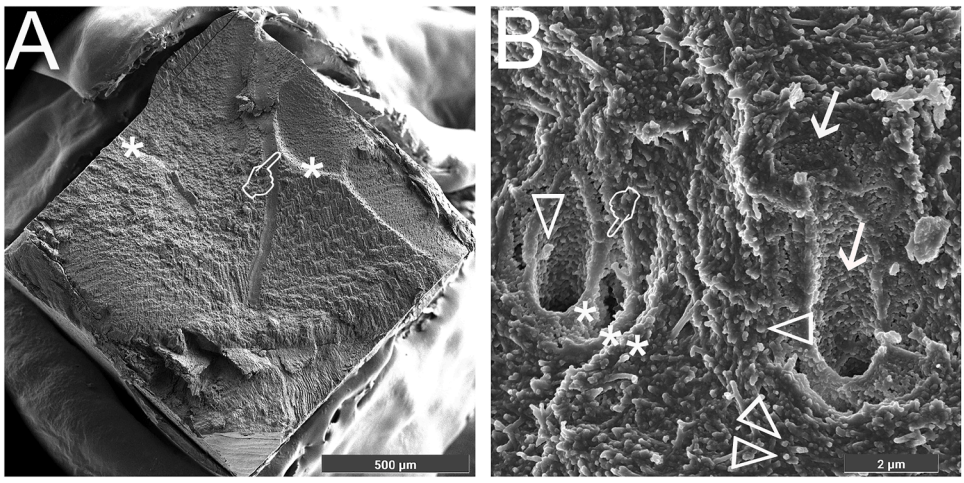

Fig. 3. SEM observations of the fractured dentin surface bonded with Zn-Dex-NPs and Single Bond adhesive (Zn-Dex-NPs group) after 21d (A, B) SBFS immersions. A, A mixed failure may be observed at the dentin surface, where dentinal tubules (asterisks) and residual adhesive resin (pointer) may be shown. B, A mixed failure with the main fracture at the bottom of the hybrid layer may be observed. Failure surface analysis permitted to observe multiple strata of mineral precipitations around the tubule wall (asterisks). Minerals formed a collar around the narrowest ring of the tubule lumen (pointer), detected below the deepest platform of crystals. Both intertubular and peritubular dentin were strongly remineralized (arrows). Magnification: (A) 400X; (B) 55,000X.

Ei (Fig. 4B). At 21d of storage time, dentin treated with undoped-NPs attained the lowest *Ei*. Dentin infiltrated with both Dex-NPs and Zn-Dex-NPs increased *Ei* after 21d of storage.

Table 2 and Figs. 5 and 6 present results from Raman analysis. After 21d, all samples showed higher mineralization degree associated to the phosphate (960cm^{-1}) and carbonate (1070cm^{-1}) bands in general terms, than that analyzed at 24 h, regardless the dentin treatment. At 24 h and 21d time point, dentin treated with Zn-Dex-NPs attained the highest phosphate (961cm^{-1}) (Fig. 5) and carbonate (1070cm^{-1}) peak intensities among groups analyzed in the present study. Samples treated with Dex-NPs did also attain the highest mineralization values (25.63) regarding the relative mineral concentrations of phosphate (RMC*p*) when compared with the rest of the groups (Table 2A). Dentin treated with Zn-Dex-NPs achieved the highest stoichiometric HAp, relative presence of mineral concerning mineral matrix (CH_2) ratio (MMR) and crystallinity (ratio 1020/1030cm^{-1}) after 21d of storage, among groups

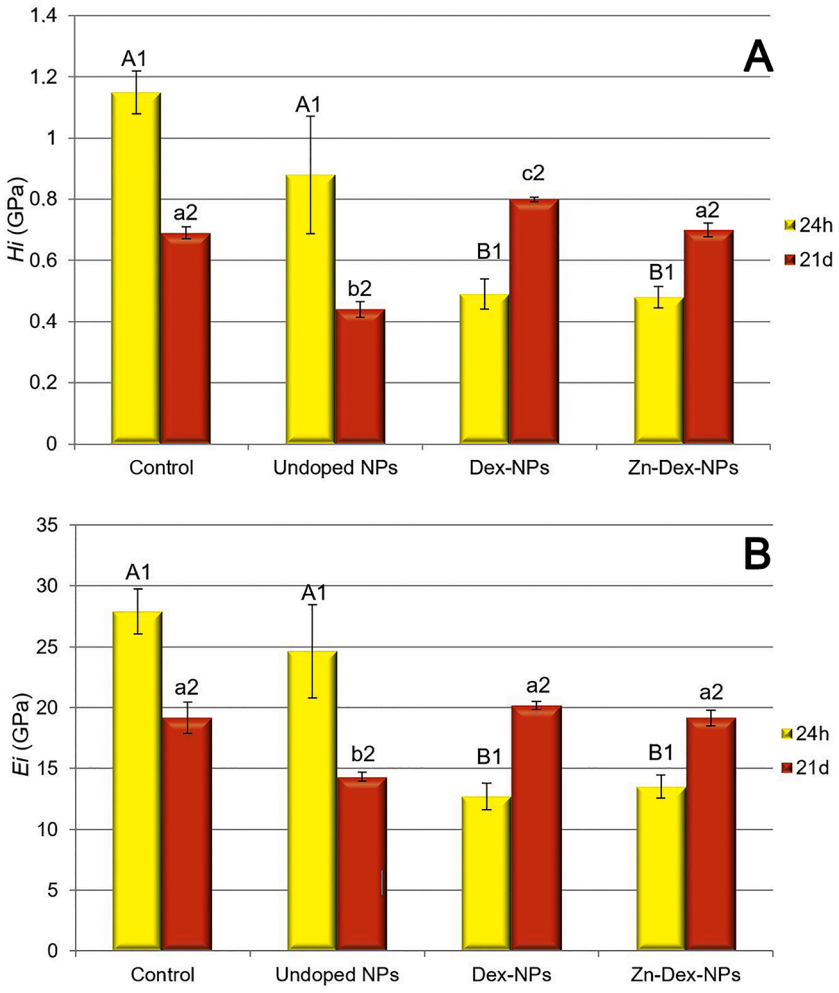

Fig. 4. Mean and standard deviation of nanohardness (*Hi*) (GPa) and Young's Modulus (*Ei*) (GPa) values at dentin surfaces of the different experimental groups. Abbreviations: NPs: undoped-nanoparticles; Dex-NPs: dexamethasone doped nanoparticles; Dex-Zn-NPs: dexamethasone and Zn doped nanoparticles. Same number indicates no significant differences between the two storage periods (24 h or 21 days) in the same treatment group. Same letter indicates no significant differences between treatment groups in the same storage period.

(872.52, 42.37 and 0.79, respectively) (Table 2A). Dentin surfaces infiltrated with Zn-Dex-NPs obtained the lowest full width at half maximum (FWHM*p*) of the phosphate (PO_4^{3-}) band at 961cm^{-1} (19.59) after 21d of storage, presenting a reduced crystallinity among groups (Table 1). On the contrary, (FWHM*c*) of the carbonate band at 1070cm^{-1} attained the highest value of amorphization (29.98) after 21d of storage, among groups (Table 1). At the spectral bands of 1032cm^{-1} (53.55), the highest values of collagen crosslinking were generated after Zn-Dex-NPs application and 21d of storage. When Dex-NPs were applied on dentin and the results were analyzed after 21d of storage, the highest values of nature and secondary structure of collagen were attained. They were measured as the molecular conformation of the collagen's polypeptide chains (Table 2B). Both Proteoglycans and phospholipids, assessed at 1062 and 1440cm^{-1} bands, respectively, attained the highest signal when Zn-Dex-NPs were applied on dentin and evaluated after 21d of storage (Table 2B). The corresponding HCA Raman images (clusters) and results (centroids) are reflected at the Fig. 6. The chemical compounds and the spatial distribution of the main spectra were revealed by HCA results and exhibited three different clustered groups in contiguous traces of the scatter plots. These results were agreeing to similar conditions of featuring, where a different color has been consigned to each cluster. Fig. 6B and 6D (undoped-NPs and Dex-NPs dentin treated, respectively) exposed a generalized higher existence of phosphate in two of the three distinct centroids (HCA_2 and HCA_3) (green and blue areas and% variances) when compared to the untreated dentin (Fig. 6A). The variance of HCA_1 increased in samples treated with Zn-Dex-NPs at 21d of storage (72%), in comparison with the untreated dentin (65%) (Fig. 6A, 6D).

4. Discusion

The use of both Dex-NPs or Zn-Dex-NPs on dentin has promoted dentin remineralization as demonstrated by testing nano-mechanical properties (Fig. 4), chemical analysis of phosphate area and peak, and so the relative concentration of mineral at 21d storage time (Table 2A). As a consequence, the null hypothesis must be rejected. These findings correlate with a gain of mineralization effect [54,55], linked to enriched precipitation of mineral (Ca and P) at the demineralized collagen [56] and to advanced functional dentin remineralization [57,58].

The mechanical properties of dentin will be affected by the degree and the quality of the mineralization. Under normal clinical conditions, the nanocrystalline hydroxyapatite is segregated into extrafibrillar and intrafibrillar mineral, supporting the later the mechanical properties performance [59]. The extrafibrilar minerals act as a granular material that can withstand load, in the absence of intrafibrilar mineralization, which is a key factor to predict biomineralization (61). Hence, the rise of both nanohardness (*Hi*) and elastic modulus (*Ei*) of the partially demineralized and infiltrated collagen is rightly linked to minerals deposits at the resin-dentin interface [60], and more concretely the intrafibrillar section [57,58]. Thus, dexamethasone seemed to favor functional mineralization and mineral deposits onto the demineralized dentin, permitting mineral precipitation in the demineralized collagen. Precipitates of mineral on the dentin surface were confirmed after infiltrating both Dex-NPs (Fig. 2B) and Zn-Dex-NPs (Fig. 3B). Shrestha et al. [15] also obtained biomineralization and an increase signals from biomarkers such as DMP-1 (dentin matrix phosphoprotein 1) and DSPP (dentin sialophosphoprotein) in stem cells from apical papilla after

Table 2
Raman intensities (arbitrary units) and ratios of mineral and organics components attained from dentin surfaces in the different experimental groups at both storage times (24 h and 21d).

A	Time	Relative Presence of Mineral							Crystallinity		
Dentin Treatment		Phosphate [961]					Carbonate [1070]		(FWHM)		[Ratio 1020/1030]
		Peak	Area	RMC (961/1003)	Stoichiometric HAp [963]	MMR (961/CH_2)	Peak	Area	Phosphate $FWHM_P$	Carbonate $FWHM_C$	
Control	24 h	713.96	18,267	29.18	640.28	25.58	87.70	3125	19.52	27.26	0.62
	21 d	715.25	18,508	21.35	684.90	28.74	88.21	3400	19.76	29.51	0.72
undoped- NPs	24 h	742.34	18,480	31.14	698.57	23.26	96.28	3418	19.00	27.16	0.55
	21 d	755.21	19,611	34.20	671.90	32.07	94.72	3193	19.82	25.78	0.62
Dex-NPs	24 h	697.79	17,963	26.57	626.44	29.91	85.62	3140	19.36	28.10	0.68
	21 d	867.27	22,597	25.63	778.29	30.97	110.09	4039	19.90	28.08	0.67
Zn-Dex NPs	24 h	787.33	19,680	23.97	829.94	28.56	107.97	3786	19.08	26.82	0.71
	21 d	925.87	23,754	25.43	872.52	42.37	116.90	4577	19.59	29.98	0.79

B	Time	Norm.	Cross-linking	Nature and secondary structure of collagen							ProteoG [1062]	PhL [1440]
Dentin Treatment		Phenyl [1003]	Pyrid [1032]	CH_2 [1450]	C-C Hy-P [871]	C—C HyL-P [920]	Collagen [937]	Amide III [1246–1270]	Amide I [1655–1667]	α-helices [1340]		
Control	24 h	24.47	39.04	27.91	19.59	34.90	95.10	43.47	2.81	8.86	67.57	18.31
	21 d	33.50	48.67	24.89	21.82	37.16	85.18	34.31	2.43	7.27	70.49	15.62
undoped-NPs	24 h	23.84	43.08	31.91	23.59	39.02	87.62	47.70	2.78	9.82	69.29	19.61
	21 d	22.08	41.42	23.55	17.93	32.65	93.09	39.88	1.44	8.62	79.54	15.76
Dex-NPs	24 h	26.26	40.62	23.33	16.19	30.95	86.32	36.50	2.39	7.21	71.09	15.40
	21 d	33.84	51.12	28.00	23.87	45.17	114.14	43.00	2.67	8.73	91.22	18.35
Zn-Dex-NPs	24 h	32.85	50.36	27.57	23.36	40.46	95.11	38.44	2.97	9.49	89.27	18.89
	21 d	36.41	53.55	21.85	19.59	40.16	102.69	32.77	2.44	7.29	91.37	19.92

Abbreviations: Time: Storage Time (24 h and 21 days); NPs: nanoparticles; Dex: Dexamethasone; RMC: Relative mineral concentration between mineral/Phenyl (1003); MMR: mineral/matrix (CH_2) ratio; AIII: Amide III (1246–1270cm^{-1}); FWHM: Full Width at Half Maximum; Norm: Normalization; Pyrid: Pyridinium; Hy-P: Hydroxyproline; HyL-P: Hydroxylated proline; DMP-1: Dentin Matrix Protein-1; ProteoG: Proteoglycans; PhL: phospholipids.For all the components, the peaks values had been normalized to the intensity of the Amide II band basis near 1510cm^{-1}. Peaks positions are expressed in cm^{-1}.

loading chitosan NPs with dexamethasone. DSPP is a matrix phosphoprotein that represents a marker of biomineralization and is strongly expressed in odontoblasts [61]. DMP-1 is a non-collagenous matrix protein present in odontoblasts and regulates biomineralization during tooth development and repair [62]. For this reason, dexamethasone may be considered as a bioactive molecule for dentin regenerative protocols [15]. Both *Hi* and *Ei* decreased in the untreated samples after 21d of immersion in SBFS, but differences disappeared when dentin surfaces were treated with NPs functionalized with dexamethasone, regardless the presence or not of Zn (Fig. 4). Differences in MTBS at both 24 h and 21d were not found (Table 1). After partial dentin demineralization when conditioning, HAp crystals remained at the tested surfaces, contributing to improve resin spreading and infiltration into the demineralized dentin [3,63,64]. In the collagen fibrils, the residual mineral might also have increased the organic matrix stability, protecting the collagen fibrils that were not entirely covered with resin [65]. Similarly, NPs, at the infiltrated interface, are able to link to this preserved collagen favoring amorphous calcium-phosphate precursors precipitates [66,67] (Figs. S2B, 2A, 2B). From this anchor position, the polymeric NPs may facilitate a controlled ion release rate, or even NPs may function as carriers of other biological compounds, allowing tissue mineralization [10], that initiate in the dentin tubules at peritubular dentin [68]. Partial demineralization by acids exposes the collagen web for remineralization, but also contributes to activate the pro-forms of dentin MMPs and other enzymes. Collagen fibrils of the scaffold can be protected from degradation by using effective inhibitors of MMPs before they can be remineralized [69]. Zinc has been demonstrated to be a potent MMPs inhibitor [26]. The increase in the percentage of both mixed and cohesive failures, over time, was also remarkable in resin-dentin interfaces containing Dex (Table 1).

After Raman analysis, these outcomes were corroborated. Multivariate analysis of Raman map images was generated by HCA (hierarchical cluster analysis) within the spectral range between 400 and 1700cm^{-1}. Multivariate data analysis in combination with Raman mapping, is a label free imaging technology for the evaluation of dentin sections. This technique differentiates cluster analysis. Thus, the HCA Raman images (clusters) and results (centroids) captured with undoped-NPs and Dex-NPs (Fig. 6B, 6C), after 21d of SBFS immersion, showed a general rise of the phosphate peak at two out the three distinguishable centroids (HCA_2 and HCA_3) (green and blue areas in Fig. 6), when compared with the samples not treated (Fig. 6A), meaning mineral gain. After 21d of SBFS storage, the increase of the phosphate peak in comparison with the control group (Table 2A) (Fig. 5B) can be, graphically, observed in the mappings contained in the Fig. 5D and 5F, (dentin treated with undoped-NPs and Dex-NPs, respectively) that reflect a greater red area, corresponding to a higher presence of phosphate [51]. The main centroid (HCA_1) (Fig. 6A, red area), which represents 65% of the variance slightly increased the intensity of the phosphate peak (7 counts) after applying Zn-Dex-NPs (72%) (Fig. 6D, red area), in the analysis at 21d time point. Micro-Raman mapping technique is, thereby, a powerful method to directly assess the resin-dentin interface's elements and their respective distribution, after the restoration placing.

A generalized increase of the phosphate peak, after applying Zn-Dex-NPs, can be seen not only at 21d storage (Figs. 5H, 6D), but at 24 h in comparison with the rest of the groups (Fig. 5G) (Table 2A). This formed mineral, when dexamethasone was present in the functionalized NPs, gave rise to Raman bands characteristics of an enriched carbonated apatite [51], in comparison with any of the groups that were tested at 21d of storage (Table 2A). Carbonated apatite is an amorphous precursor of HAp [51], providing not only high instability and solubility to the new mineral, but also an outstanding source of ions for further dentin remineralization [21]. The increased degree of carbonate substitution in the lattice structure of apatite correlates with the presence of a prominent carbonate band around 1070cm^{-1} [70], and coincides with

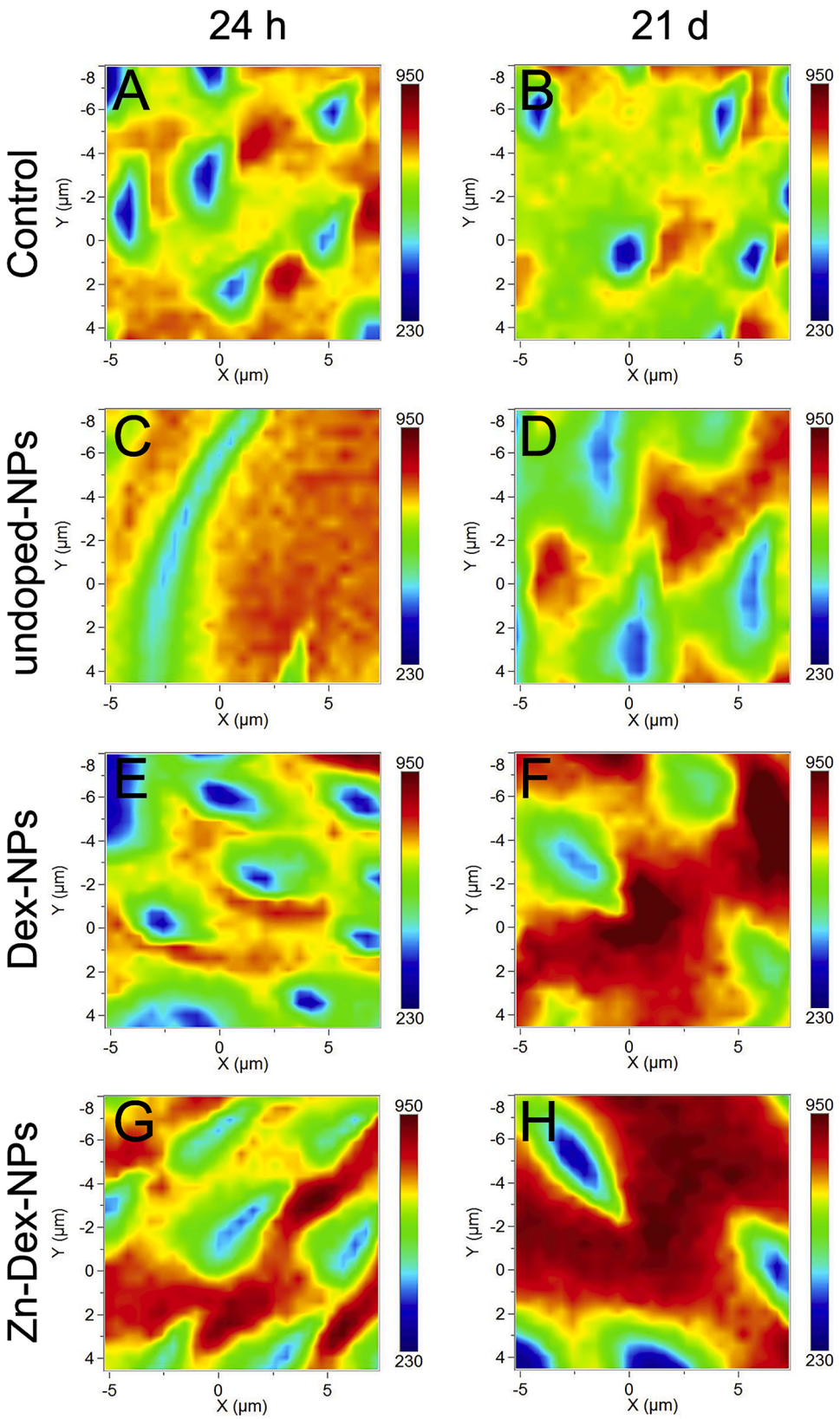

Fig. 5. 2D micro-Raman map of phosphate peak intensities ($961cm^{-1}$) on dentin surfaces: the left column shows dentin surfaces after 24 h storage, (A) untreated dentin, (C) treated with undoped-Nps, (E) Dex-NPs and (G) Zn-Dex-NPs. The right column shows dentin surfaces stored for 21 days, (B) untreated dentin, (D) treated dentin with undoped-Nps, (F) Dex-NPs and (H) Zn-Dex-NPs.

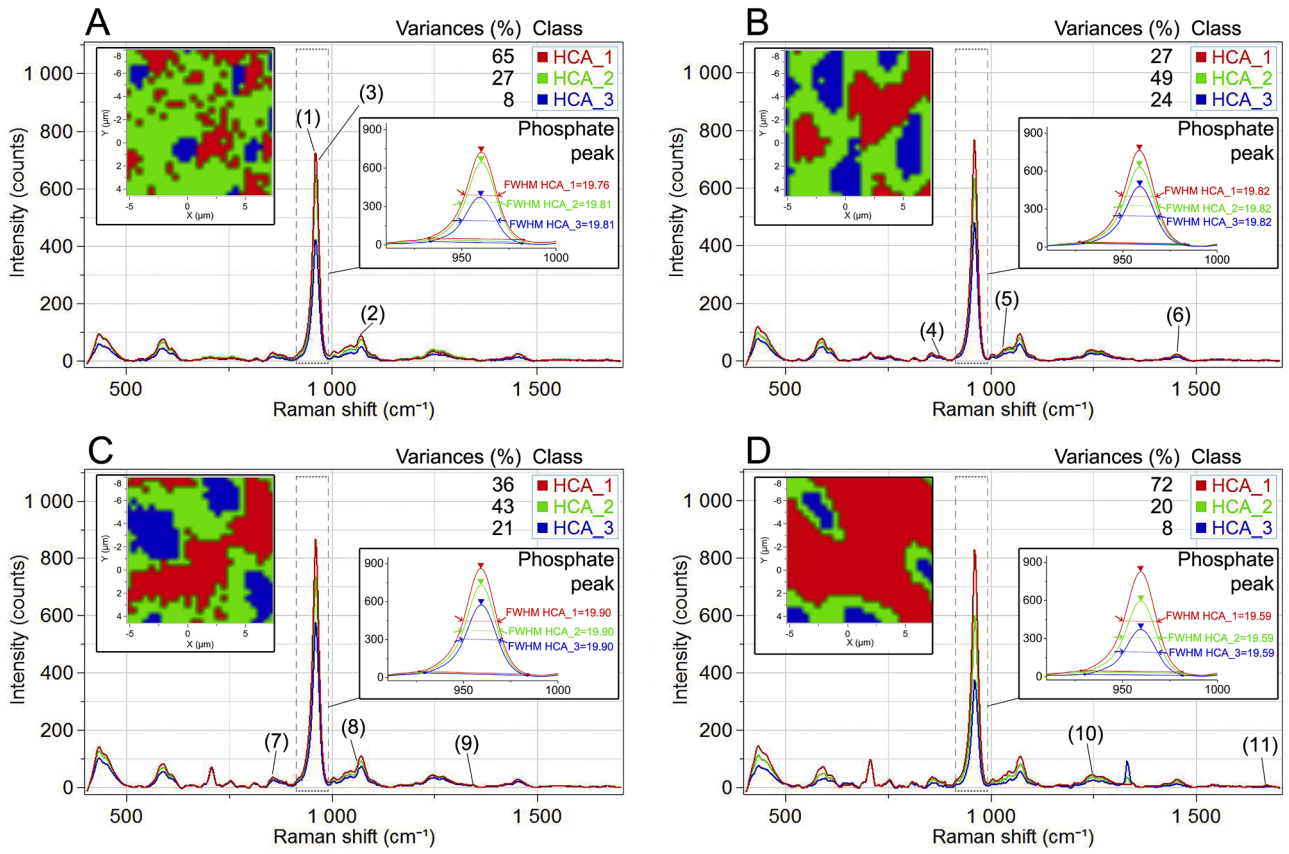

Fig. 6. Raman spectra from hierarchical cluster analysis (HCA) results of untreated dentin (A), dentin treated with undoped-NPs (B), Dex-NPs (C) and Zn-Dex-NPs (D) after 21d storage. The peaks position are marked with the numbers in parenthesis: (1) phosphate *v1* (961cm^{-1}); (2) carbonate (1070cm^{-1}); (3) Stoichiometric HAp (963cm^{-1}); (4) C—C Hydroxyproline (871cm^{-1}); (5) pyridinium (1032cm^{-1}); (6) CH_2 (1450cm^{-1}); (7) Collagen (937cm^{-1}); (8) Proteoglycans (1062cm^{-1}); (9) α-helices (1340cm^{-1}); (10) Amide III (1246–1270cm^{-1}) and (11) Amide I (1655–1667cm^{-1}). Top left insets are showing the color mapping from Hierarchical Cluster Analysis (HCA) images. Three levels of HCA clustering are shown. Areas of distinct colors have differences in Raman spectral distribution and chemical composition. Each cluster is assigned to a different color (red, green and blue). Right insets are showing Full Width Half Maximum (FWHM) of the phosphate peak (961cm^{-1}) at single truncated spectra points.

the narrowing full-width half-maximum (FWHM) of the phosphate ν_1 peak (at ca. 961cm^{-1}), when zinc was used in NPs functionalization (Table 2A). FWHM reflects a broad augmentation of crystallographic maturity, crystallinity, in minerals [40], at the dentin surface treated with Zn-Dex-NPs (Table 2A), and was evidenced at Fig. 6D. High crystallinity usually became associated to, *i)* the great phosphate ν_1 vibration, at 963 cm^{-1} height [71] (Table 2A) which corresponded to stoichiometric HAp, with increased maturity [41,50]. Advanced maturity and hard tissue healing with biomineralization were also reflected in the highest peaks obtained after observing the phospholipid peaks (1440cm^{-1}), corresponding to samples treated with Zn-Dex-NPs (Table 2B). Hence, the association between high crystallinity and good mechanical properties, has been confirmed in the present research (Table 2A, Fig. 4).

Both Dex-NPs and Zn-Dex-NPs contributed to the improvement of the secondary structure and nature of collagen in dentin when compared with samples both untreated and treated with undoped-NPs, after 21d storage time (Table 2B). This rise of values indicated better organization, recovery [72], collagen quality and improved structural differences [70]. At the long term, Dex-NPs and Zn-Dex-NPs application would favor advanced mineralization, because of the increase of collagen cross-linking [73], as pyridinium (1032cm^{-1}) increased at 21d when compared with the rest of the groups (Table 2B). Raman analysis have also shown that proteoglycans increased in the different groups of study following the trend: untreated dentin < dentin treated with undoped-NPs < dentin treated with Dex-NPs < dentin treated with Zn-Dex-NPs. Between continuous collagen fibrils, proteoglycans have been proposed to act as bridges, thus indirectly facilitating the deposition of the extrafibrillar apatite in mineralized tissues [52]. Therefore, it can be inferred that the higher signals corresponding to proteoglycans may be associated to an increase of mineralization after applying Zn-Dex-NPs on dentin due to the roll of the highly negatively charged glycosaminoglycan side chains in attracting calcium ions, conducting to a biological signaling role [74,75]. The ability of tissues to receive, process, and transmit signals with its environment and with itself is understood as signaling pathway [76,77].

A feasible option to obtain coronal dentin remineralization is the application of Dex-NPs and Zn-Dex-NPs, as they produce mineral deposits in dentin (Figs. 2B, 3B, respectively) and the reinforcement of its structure (Fig. 4). Besides, it should be considered that non-released dexamethasone and/or Zn that may have remained linked to NPs might also continue to be bioactive. Additional research on using Dex-doped nanoparticles in endodontics is encouraged. This experiment gathers some limitations. In order to include morpho-physico-chemically evaluation of these treated surfaces, X-ray fluorescence microscopy studies and X-ray micro-computed tomography analysis should be implemented. Combining doxycycline loaded NPs with Dex-NPs could pose a future challenge for a remineralizing, antimicrobial, and anti-inflammatory therapy in root canal dentin. MMPs-mediated collagen degradation will also be determined in the next strategy of research when using both doxycycline and dexamethasone-doped NPs on dentin surfaces.

5. Conclusions

The application and further infiltration on dentin of polymeric nanoparticles doped with dexamethasone has promoted functional remineralization as proved by nanohardness, modulus of Young testing and Raman analysis. These new minerals showed better crystallographic maturity, crystallinity and amorphization than those formed on dentin treated with unloaded nanoparticles. Functionalization with both dexamethasone and zinc improved the nature and secondary structure of dentin collagen, providing better organization, and granting advanced structural differences and collagen quality respect to the dentin groups treated with the unloaded nanoparticles.

Credit author statement

Manuel Toledano: Conceptualization, Formal analysis, Funding acquisition, Investigation, Methodology, Project administration, Supervision, Visualization, Validation, Writing – original draft and review & editing. Estrella Osorio: Investigation, Methodology, Data curation, Visualization, Software, Resources, Writing – original draft and review & editing. María T. Osorio: Methodology (Nanoparticles fabrication and characterization), Investigation, Visualization, Writing – review & editing (English translation and correction). Fátima S. Aguilera: Data curation, Investigation, Methodology (adhesion protocol), Visualization, Writing – original draft and review & editing. Raquel Toledano: Data curation, Investigation, Methodology (Nanoparticles fabrication and characterization), Visualization, Writing – review & editing (English translation and correction). Enrique Fernández: Methodology (Size and Z-potential measurements; sample preparation for MTBS). Data curation, Visualization, Writing – review & editing. Raquel Osorio: Conceptualization, Formal analysis, Funding acquisition, Investigation, Methodology, Project administration, Supervision, Visualization, Writing – original draft.

Declaration of Competing Interest

The authors declare that they have no known competing financial interests or personal relationships that could have appeared to influence the work reported in this paper.

Acknowledgements

The present study was supported by Grant PID2020-114694RB-I00 funded by MCIN/AEI 10.13039/501100011033. Funding for open access charge: Universidad de Granada / CBUA.

Supplementary materials

Supplementary material associated with this article can be found, in the online version, at doi:10.1016/j.jdent.2023.104447.

References

[1] J.M. Guo, P. Makvandi, C.C. Wei, J.H. Chen, H.K. Xu, L. Breschi, D.H. Pashley, C. Huang, L.N. Niu, F.R. Tay, Polymer conjugation optimizes EDTA as a calcium-chelating agent that exclusively removes extrafibrillar minerals from mineralized collagen, Acta Biomater. 90 (2019) 424–440, https://doi.org/10.1016/j.actbio.2019.04.011.

[2] N. Nakabayashi, The hybrid layer: a resin-dentin composite, Proc. Finn. Dent. Soc. 88 (Suppl 1) (1992) 321–329.

[3] R. Frankenberger, J. Sindel, N. Krämer, A. Petschelt, Dentin bond strength and marginal adaptation: direct composite resins vs ceramic inlays, Oper. Dent. 24 (1999) 147–155.

[4] Y. Wang, P. Spencer, Hybridization efficiency of the adhesive/dentin interface with wet bonding, J. Dent. Res. 82 (2003) 141–145, https://doi.org/10.1177/154405910308200213.

[5] A. Misra, P. Spencer, O. Marangos, Y. Wang, J.L. Katz, Micromechanical analysis of dentin/adhesive interface by the finite element method, J. Biomed. Mater. Res. Part B Appl. Biomater. 70 (2004) 56–65, https://doi.org/10.1002/jbm.b.30012.

[6] D.H. Pashley, F.R. Tay, C. Yiu, M. Hashimoto, L. Breschi, R.M. Carvalho, S. Ito, Collagen degradation by host-derived enzymes during aging, J. Dent. Res. 83 (2004) 216–221, https://doi.org/10.1177/154405910408300306.

[7] R. Osorio, M. Yamauti, E. Osorio, M.E. Ruiz-Requena, D. Pashley, F. Tay, M. Toledano, Effect of dentin etching and chlorhexidine application on metalloproteinase-mediated collagen degradation, Eur. J. Oral Sci. 119 (2011) 79–85, https://doi.org/10.1111/j.1600-0722.2010.00789.x.

[8] M. Yoshiyama, A. Urayama, T. Kimochi, T. Matsuo, D.H. Pashley, Comparison of conventional vs self-etching adhesive bonds to caries-affected dentin, Oper. Dent. 25 (2000) 163–169.

[9] R. Osorio, I. Cabello, A.L. Medina-Castillo, E. Osorio, M. Toledano, Zinc-modified nanopolymers improve the quality of resin–dentin bonded interfaces, Clin. Oral Invest. 20 (2016) 2411–2420, https://doi.org/10.1007/s00784-016-1738-y.

[10] M. Toledano, M. Vallecillo-Rivas, F.S. Aguilera, M.T. Osorio, E. Osorio, R. Osorio, Polymeric zinc-doped nanoparticles for high performance in restorative dentistry, J. Dent. 107 (2021), 103616, https://doi.org/10.1016/j.jdent.2021.103616.

[11] C. Wu, Y. Zhang, W. Fan, X. Ke, X. Hu, Y. Zhou, Y. Xiao, CaSiO3 microstructure modulating the in vitro and in vivo bioactivity of poly(lactide-co-glycolide) microspheres, J. Biomed. Mater. Res.Part A 98A (2011) 122–131, https://doi.org/10.1002/jbm.a.33092.

[12] E.V.F. Fachin, R.K. Scarparo, A.P.W. Pezzi, S.B. Luisi, M. Sant'ana, Effect of betamethasone on the pulp after topical application to the dentin of rat teeth: vascular aspects of the inflammation, J. Appl. Oral Sci. 17 (2009) 335–339, https://doi.org/10.1590/S1678-77572009000400012.

[13] A. Alagha, A. Nourallah, S. Alhariri, Dexamethasone- loaded polymeric porous sponge as a direct pulp capping agent, J. Biomater. Sci. 31 (2020) 1689–1705, https://doi.org/10.1080/09205063.2020.1769801. Polymer Edition.

[14] H.C. Lim, O.H. Nam, M. Kim, A. El-Fiqi, H.M. Yun, Y.M. Lee, G.Z. Jin, H.H. Lee, H. W. Kim, E.C. Kim, Delivery of dexamethasone from bioactive nanofiber matrices stimulates odontogenesis of human dental pulp cells through integrin/BMP/mTOR signaling pathways, IJN 11 (2016) 2557–2567, https://doi.org/10.2147/IJN.S97846.

[15] S. Shrestha, C.D. Torneck, A. Kishen, Dentin conditioning with bioactive molecule releasing nanoparticle system enhances adherence, viability, and differentiation of stem cells from apical papilla, J. Endod. 42 (2016) 717–723, https://doi.org/10.1016/j.joen.2016.01.026.

[16] R. Furseth, I.A. Mjör, The fine structure of corticosteroid-covered, human dentine, Arch. Oral Biol. 17 (1972), https://doi.org/10.1016/0003-9969(72)90198-7, 719-IN23.

[17] A. Martins, A.R.C. Duarte, S. Faria, A.P. Marques, R.L. Reis, N.M. Neves, Osteogenic induction of hBMSCs by electrospun scaffolds with dexamethasone release functionality, Biomaterials 31 (2010) 5875–5885, https://doi.org/10.1016/j.biomaterials.2010.04.010.

[18] S. Ding, J. Li, C. Luo, L. Li, G. Yang, S. Zhou, Synergistic effect of released dexamethasone and surface nanoroughness on mesenchymal stem cell differentiation, Biomater. Sci. 1 (2013) 1091–1100, https://doi.org/10.1039/C3BM60095E.

[19] K. Qiu, B. Chen, W. Nie, X. Zhou, W. Feng, W. Wang, L. Chen, X. Mo, Y. Wei, C. He, Electrophoretic deposition of dexamethasone-loaded mesoporous silica nanoparticles onto poly(l-Lactic Acid)/Poly(ε-Caprolactone) composite scaffold for bone tissue engineering, ACS Appl. Mater. Interfaces 8 (2016) 4137–4148, https://doi.org/10.1021/acsami.5b11879.

[20] M. Toledano-Osorio, R. Osorio, F.S. Aguilera, A.L. Medina-Castillo, M. Toledano, E. Osorio, S. Acosta, R. Chen, C. Aparicio, Polymeric nanoparticles protect the resin-dentin bonded interface from cariogenic biofilm degradation, Acta Biomater. 111 (2020) 316–326, https://doi.org/10.1016/j.actbio.2020.05.002.

[21] M. Toledano, F.S. Aguilera, E. Osorio, M. Toledano-Osorio, G. Escames, A. L. Medina-Castillo, R. Toledano, C.D. Lynch, R. Osorio, Melatonin-doped polymeric nanoparticles reinforce and remineralize radicular dentin: morpho-histological, chemical and biomechanical studies, Dent. Mater. 37 (2021) 1107–1120, https://doi.org/10.1016/j.dental.2021.03.007.

[22] M. Toledano-Osorio, F.S. Aguilera, E. Muñoz-Soto, E. Osorio, M. Toledano, G. Escames, A.L. Medina-Castillo, M.T. Osorio, M.T. López-López, M. Vallecillo-Rivas, R. Osorio, Melatonin-doped polymeric nanoparticles induce high crystalline apatite formation in root dentin, Dent. Mater. 37 (2021) 1698–1713, https://doi.org/10.1016/j.dental.2021.09.001.

[23] M. Toledano, E. Osorio, F.S. Aguilera, E. Muñoz-Soto, M. Toledano-Osorio, M. T. López-López, A.L. Medina-Castillo, Á. Carrasco-Carmona, R. Osorio, Polymeric nanoparticles for endodontic therapy, J. Mech. Behav. Biomed. Mater. 103 (2020), 103606, https://doi.org/10.1016/j.jmbbm.2019.103606.

[24] A. Hoppe, N.S. Güldal, A.R. Boccaccini, A review of the biological response to ionic dissolution products from bioactive glasses and glass-ceramics, Biomaterials 32 (2011) 2757–2774, https://doi.org/10.1016/j.biomaterials.2011.01.004.

[25] M. Toledano, S. Sauro, I. Cabello, T. Watson, R. Osorio, A Zn-doped etch-and-rinse adhesive may improve the mechanical properties and the integrity at the bonded-dentin interface, Dent. Mater. 29 (2013) e142–e152, https://doi.org/10.1016/j.dental.2013.04.024.

[26] R. Osorio, M. Yamauti, E. Osorio, M.E. Ruiz-Requena, D.H. Pashley, F. Tay, M. Toledano, Zinc reduces collagen degradation in demineralized human dentin explants, J. Dent. 39 (2011) 148–153, https://doi.org/10.1016/j.jdent.2010.11.005.

[27] T. Takatsuka, K. Tanaka, Y. Iijima, Inhibition of dentine demineralization by zinc oxide: in vitro and in situ studies, Dent. Mater. 21 (2005) 1170–1177, https://doi.org/10.1016/j.dental.2005.02.006.

[28] I. Mayer, F. Apfelbaum, J.D.B. Featherstone, Zinc ions in synthetic carbonated hydroxyapatites, Arch. Oral Biol. 39 (1994) 87–90, https://doi.org/10.1016/0003-9969(94)90040-X.
[29] P. Fratzl, H.S. Gupta, E.P. Paschalis, P. Roschger, Structure and mechanical quality of the collagen– mineral nano-composite in bone, J. Mater. Chem. 14 (2004) 2115–2123, https://doi.org/10.1039/B402005G.
[30] J.H. Kinney, R.K. Nalla, J.A. Pople, T.M. Breunig, R.O. Ritchie, Age-related transparent root dentin: mineral concentration, crystallite size, and mechanical properties, Biomaterials 26 (2005) 3363–3376, https://doi.org/10.1016/j.biomaterials.2004.09.004.
[31] B. Poon, D. Rittel, G. Ravichandran, An analysis of nanoindentation in linearly elastic solids, Int. J. Solids Struct. 45 (2008) 6018–6033, https://doi.org/10.1016/j.ijsolstr.2008.07.021.
[32] H. Milly, F. Festy, T.F. Watson, I. Thompson, A. Banerjee, Enamel white spot lesions can remineralise using bio-active glass and polyacrylic acid-modified bio-active glass powders, J. Dent. 42 (2014) 158–166, https://doi.org/10.1016/j.jdent.2013.11.012.
[33] A.L. Medina-Castillo, Thermodynamic principles of precipitation polymerization and role of fractal nanostructures in the particle size control, Macromolecules 53 (2020) 5687–5700, https://doi.org/10.1021/acs.macromol.0c00973.
[34] S.R. Schaffazick, A.R. Pohlmann, G. Mezzalira, S.S. Guterres, Development of nanocapsule suspensions and nanocapsule spray-dried powders containing melatonin, J. Braz. Chem. Soc. 17 (2006) 562–569, https://doi.org/10.1590/S0103-50532006000300020.
[35] F. Noori Siahdasht, N. Farhadian, M. Karimi, L. Hafizi, Enhanced delivery of melatonin loaded nanostructured lipid carriers during in vitro fertilization: NLC formulation, optimization and IVF efficacy, RSC Adv. 10 (2020) 9462–9475, https://doi.org/10.1039/C9RA10867J.
[36] C. Rodriguez-Navarro, A. Burgos Cara, K. Elert, C.V. Putnis, E. Ruiz-Agudo, Direct nanoscale imaging reveals the growth of calcite crystals via amorphous nanoparticles, Cryst. Growth Des. 16 (2016) 1850–1860, https://doi.org/10.1021/acs.cgd.5b01180.
[37] H. Ryou, L.N. Niu, L. Dai, C.R. Pucci, D.D. Arola, D.H. Pashley, F.R. Tay, Effect of biomimetic remineralization on the dynamic nanomechanical properties of dentin hybrid layers, J. Dent. Res. 90 (2011) 1122–1128, https://doi.org/10.1177/0022034511414059.
[38] W.C. Oliver, G.M. Pharr, An improved technique for determining hardness and elastic modulus using load and displacement sensing indentation experiments, J. Mater. Res. 7 (1992) 1564–1583, https://doi.org/10.1557/JMR.1992.1564.
[39] K. Karan, X. Yao, C. Xu, Y. Wang, Chemical profile of the dentin substrate in non-carious cervical lesions, Dent. Mater. 25 (2009) 1205–1212, https://doi.org/10.1016/j.dental.2009.04.006.
[40] A.G. Schwartz, J.D. Pasteris, G.M. Genin, T.L. Daulton, S. Thomopoulos, Mineral distributions at the developing tendon enthesis, PLoS One 7 (2012) e48630, https://doi.org/10.1371/journal.pone.0048630.
[41] J.A. Timlin, A. Carden, M.D. Morris, R.M. Rajachar, D.H. Kohn, Raman spectroscopic imaging markers for fatigue-related microdamage in bovine bone, Anal. Chem. 72 (2000) 2229–2236, https://doi.org/10.1021/ac9913560.
[42] Y. Wang, X. Yao, Morphological/chemical imaging of demineralized dentin layer in its natural, wet state, Dent. Mater. 26 (2010) 433–442, https://doi.org/10.1016/j.dental.2010.01.002.
[43] D. Magne, P. Weiss, J.M. Bouler, O. Laboux, G. Daculsi, Study of the maturation of the organic (type I collagen) and mineral (nonstoichiometric apatite) constituents of a calcified tissue (dentin) as a function of location: a Fourier transform infrared microspectroscopic investigation, J. Bone Miner. Res. 16 (2001) 750–757, https://doi.org/10.1359/jbmr.2001.16.4.750.
[44] C. Xu, Y. Wang, Cross-linked demineralized dentin maintains its mechanical stability when challenged by bacterial collagenase, J. Biomed. Mater. Res. Part B Appl. Biomater. 96B (2011) 242–248, https://doi.org/10.1002/jbm.b.31759.
[45] U. Daood, K. Iqbal, L.I. Nitisusanta, A.S. Fawzy, Effect of chitosan/riboflavin modification on resin/dentin interface: spectroscopic and microscopic investigations, J. Biomed. Mater. Res. A 101 (2013) 1846–1856, https://doi.org/10.1002/jbm.a.34482.
[46] M. Jastrzebska, R. Wrzalik, A. Kocot, J. Zalewska-Rejdak, B. Cwalina, Raman spectroscopic study of glutaraldehyde-stabilized collagen and pericardium tissue, J. Biomater. Sci. 14 (2003) 185–197, https://doi.org/10.1163/156856203321142605. Polymer Edition.
[47] C. Xu, Y. Wang, Collagen cross linking increases its biodegradation resistance in wet dentin bonding, J. Adhes. Dent. 14 (2012) 11–18, https://doi.org/10.3290/j.jad.a21494.
[48] R. Vanna, P. Ronchi, A.T.M. Lenferink, C. Tresoldi, C. Morasso, D. Mehn, M. Bedoni, S. Picciolini, L.W.M.M. Terstappen, F. Ciceri, C. Otto, F. Gramatica, Label-free imaging and identification of typical cells of acute myeloid leukaemia and myelodysplastic syndrome by Raman microspectroscopy, Analyst 140 (2015) 1054–1064, https://doi.org/10.1039/C4AN02127D.
[49] J. Garcia-Guinea, A. Jorge, L. Tormo, M. Furio, E. Crespo-Feo, V. Correcher, P. Prado-Herrero, A.C. Soria, J. Sanz, J.L. Nieves-Aldrey, Ossification vesicles with calcium phosphate in the eyes of the insect copium teucrii (Hemiptera: tingidae), Sci. World J. 11 (2011) 186–198, https://doi.org/10.1100/tsw.2011.9.
[50] A. Kunstar, J. Leijten, S. van Leuveren, J. Hilderink, C. Otto, C.A. van Blitterswijk, M. Karperien, A.A. van Apeldoorn, Recognizing different tissues in human fetal femur cartilage by label-free Raman microspectroscopy, J. Biomed. Opt. 17 (2012), 116012, https://doi.org/10.1117/1.JBO.17.11.116012.
[51] C. Wang, Y. Wang, N.T. Huffman, C. Cui, X. Yao, S. Midura, R.J. Midura, J. P. Gorski, Confocal laser Raman microspectroscopy of biomineralization Foci in UMR 106 osteoblastic cultures reveals temporally synchronized protein changes preceding and accompanying mineral crystal deposition, J. Biol. Chem. 284 (2009) 7100–7113, https://doi.org/10.1074/jbc.M805898200.
[52] K. Stankoska, L. Sarram, S. Smith, A. Bedran-Russo, C. Little, M. Swain, L. Bertassoni, Immunolocalization and distribution of proteoglycans in carious dentine, Aust. Dent. J. 61 (2016) 288–297, https://doi.org/10.1111/adj.12376.
[53] G. Penel, C. Delfosse, M. Descamps, G. Leroy, Composition of bone and apatitic biomaterials as revealed by intravital Raman microspectroscopy, Bone 36 (2005) 893–901, https://doi.org/10.1016/j.bone.2005.02.012.
[54] M. Toledano, R. Osorio, E. Osorio, A.L. Medina-Castillo, M. Toledano-Osorio, F. S. Aguilera, Ions-modified nanoparticles affect functional remineralization and energy dissipation through the resin-dentin interface, J. Mech. Behav. Biomed. Mater. 68 (2017) 62–79, https://doi.org/10.1016/j.jmbbm.2017.01.026.
[55] R. Osorio, E. Osorio, F.S. Aguilera, A.L. Medina-Castillo, M. Toledano, M. Toledano-Osorio, Silver improves collagen structure and stability at demineralized dentin: a dynamic-mechanical and Raman analysis, J. Dent. 79 (2018) 61–67, https://doi.org/10.1016/j.jdent.2018.10.003.
[56] M.D. McKee, Y. Nakano, D.L. Masica, J.J. Gray, I. Lemire, R. Heft, M.P. Whyte, P. Crine, J.L. Millán, Enzyme replacement therapy prevents dental defects in a model of hypophosphatasia, J. Dent. Res. 90 (2011) 470–476, https://doi.org/10.1177/0022034510393517.
[57] M. Balooch, S. Habelitz, J.H. Kinney, S.J. Marshall, G.W. Marshall, Mechanical properties of mineralized collagen fibrils as influenced by demineralization, J. Struct. Biol. 162 (2008) 404–410, https://doi.org/10.1016/j.jsb.2008.02.010.
[58] L.E. Bertassoni, S. Habelitz, J.H. Kinney, S.J. Marshall, G.W. Marshall, Biomechanical perspective on the remineralization of dentin, Caries Res. 43 (2009) 70–77, https://doi.org/10.1159/000201593.
[59] J.H. Kinney, S. Habelitz, S.J. Marshall, G.W. Marshall, The importance of intrafibrillar mineralization of collagen on the mechanical properties of dentin, J. Dent. Res. 82 (2003) 957–961, https://doi.org/10.1177/154405910308201204.
[60] Y. Li, T.T. Thula, S. Jee, S.L. Perkins, C. Aparicio, E.P. Douglas, L.B. Gower, Biomimetic mineralization of woven bone-like nanocomposites: role of collagen cross-links, Biomacromolecules 13 (2012) 49–59, https://doi.org/10.1021/bm201070g.
[61] C. Qin, J.C. Brunn, E. Cadena, A. Ridall, H. Tsujigiwa, H. Nagatsuka, N. Nagai, W. T. Butler, The expression of dentin sialophosphoprotein gene in bone, J. Dent. Res. 81 (2002) 392–394, https://doi.org/10.1177/154405910208100607.
[62] A. Almushayt, K. Narayanan, A.E. Zaki, A. George, Dentin matrix protein 1 induces cytodifferentiation of dental pulp stem cells into odontoblasts, Gene Ther. 13 (2006) 611–620, https://doi.org/10.1038/sj.gt.3302687.
[63] T. Saito, M. Yamauchi, M.A. Crenshaw, Apatite induction by insoluble dentin collagen, J. Bone Miner. Res. 13 (1998) 265–270, https://doi.org/10.1359/jbmr.1998.13.2.265.
[64] M. Toledano, E. Osorio, I. Cabello, R. Osorio, Early dentine remineralisation: morpho-mechanical assessment, J. Dent. 42 (2014) 384–394, https://doi.org/10.1016/j.jdent.2014.01.012.
[65] S. Sauro, F. Mannocci, M. Toledano, R. Osorio, D.H. Pashley, T.F. Watson, EDTA or H3PO4/NaOCl dentine treatments may increase hybrid layers' resistance to degradation: a microtensile bond strength and confocal-micropermeability study, J. Dent. 37 (2009) 279–288, https://doi.org/10.1016/j.jdent.2008.12.002.
[66] T. Karakida, K. Onuma, M.M. Saito, R. Yamamoto, T. Chiba, R. Chiba, Y. Hidaka, K. Fujii-Abe, H. Kawahara, Y. Yamakoshi, Potential for drug repositioning of midazolam for dentin regeneration, Int. J. Mol. Sci. 20 (2019) 670, https://doi.org/10.3390/ijms20030670.
[67] R.N. Salaie, A. Besinis, H. Le, C. Tredwin, R.D. Handy, The biocompatibility of silver and nanohydroxyapatite coatings on titanium dental implants with human primary osteoblast cells, Mater. Sci. Eng. C 107 (2020), 110210, https://doi.org/10.1016/j.msec.2019.110210.
[68] K. Yoshihara, N. Nagaoka, A. Nakamura, T. Hara, S. Hayakawa, Y. Yoshida, B. Van Meerbeek, Three-dimensional observation and analysis of remineralization in dentinal caries lesions, Sci. Rep. 10 (2020) 4387, https://doi.org/10.1038/s41598-020-61111-1.
[69] Y. Liu, S. Mai, N. Li, C.K.Y. Yiu, J. Mao, D.H. Pashley, F.R. Tay, Differences between top-down and bottom-up approaches in mineralizing thick, partially demineralized collagen scaffolds, Acta Biomater. 7 (2011) 1742–1751, https://doi.org/10.1016/j.actbio.2010.11.028.
[70] H. Salehi, E. Terrer, I. Panayotov, B. Levallois, B. Jacquot, H. Tassery, F. Cuisinier, Functional mapping of human sound and carious enamel and dentin with Raman spectroscopy, J. Biophotonics 6 (2013) 765–774, https://doi.org/10.1002/jbio.201200095.
[71] R. Osorio, E. Osorio, I. Cabello, M. Toledano, Zinc induces apatite and scholzite formation during dentin remineralization, Caries Res. 48 (2014) 276–290, https://doi.org/10.1159/000356873.
[72] L.K. Bakland, J.O. Andreasen, Will mineral trioxide aggregate replace calcium hydroxide in treating pulpal and periodontal healing complications subsequent to dental trauma? A review, Dent. Traumatol. 28 (2012) 25–32, https://doi.org/10.1111/j.1600-9657.2011.01049.x.
[73] M. Toledano, F.S. Aguilera, E. Osorio, I. Cabello, M. Toledano-Osorio, R. Osorio, Functional and molecular structural analysis of dentine interfaces promoted by a Zn-doped self-etching adhesive and an in vitro load cycling model, J. Mech. Behav. Biomed. Mater. 50 (2015) 131–149, https://doi.org/10.1016/j.jmbbm.2015.05.026.
[74] L.E. Bertassoni, K. Stankoska, M.V. Swain, Insights into the structure and composition of the peritubular dentin organic matrix and the lamina limitans, Micron 43 (2012) 229–236, https://doi.org/10.1016/j.micron.2011.08.003.

[75] J.H. Kinney, G.W. Marshall, S.J. Marshall, Three-dimensional mapping of mineral densities in carious dentin: theory and method, Scanning Microsc. 8 (1994). https://digitalcommons.usu.edu/microscopy/vol8/iss2/6.

[76] J.D. Jordan, E.M. Landau, R. Iyengar, Signaling networks: the origins of cellular multitasking, Cell 103 (2000) 193–200.

[77] Neitzel, J., Rasband, M. Cell communication, learn science at scitable (Nature). (2014). https://www.nature.com/scitable/topic/cell-communication-14122659/.